



# Image-based method for the angular vibration measurement of a linear array camera

XUE ZHI-PENG,<sup>1,2,\*</sup> WANG CHAO,<sup>1,2</sup> LI MING,<sup>1,2</sup> WANG CHUNXUE,<sup>2</sup> JIA HONGGUANG,<sup>1,2</sup> AND YU YUE<sup>1,2,3</sup>

<sup>1</sup>Chang Guang Satellite Technology Company, 1299, Mingxi Road, BeiHu Science and Technology Development District, Changchun 130102, China

<sup>2</sup>Changchun Institute of Optics, Fine Mechanics and Physics, Chinese Academy of Sciences, 3888, Dong Nanhu Road, Changchun 130033, China

<sup>3</sup>University of Chinese Academy of Sciences, 19, A Yuquan Road, Beijing 100049, China

\*Corresponding author: xuezhipeengs1314@126.com

Received 29 October 2020; revised 24 December 2020; accepted 26 December 2020; posted 4 January 2021 (Doc. ID 413355); published 28 January 2021

Measurements of angular vibration of aerial cameras in a variety of operating conditions are critical to analyze the performance of the vibration isolation system. Instead of using an additional optical system to measure the angular motion of the camera, an image-based and easy-to-implement method is proposed for the linear array camera to measure the image motions captured by the camera directly. The natural frequencies of the vibration isolation were also measured by laboratory vibration test. For image vibration measuring, the angular vibration is represented in image motion by the relationship between the image motion and angular motion of the camera. Based on the pushbroom imaging principle, the image motion at the edge of the foreground image of the linear object is extracted using image processing technology including image segment and edge detection methods. Then the image motion is analyzed in the time and frequency domains. The proposed method has been successfully demonstrated for the angular vibration measurement by a flight test. The results of the vibration sensors and the position and orientation system of the flight tests are also given to validate the effectiveness and accuracy of the proposed approach. © 2021 Optical Society of America

<https://doi.org/10.1364/AO.413355>

## 1. INTRODUCTION

Pushbroom scanners with linear image sensors are generally used in observation aerial systems. The use of such scanners allows reduction of the size and cost of the image payload. However, it is critical that the camera system requires high stability of the airplane or unmanned aerial vehicle (UAV) during scanning of the frame. For a high-precision aerial linear array camera, the optimal stabilization is achieved when vibrations of any type in the entire amplitude and frequency spectrum can be isolated or compensated for. Windau *et al.* [1] introduced a multilayer real-time video image stabilization system for aerial robots including inertial measurement unit, mechanical vibration isolation, optical image stabilization, and digital video stabilization system.

Performance of high-resolution remote sensing payloads is often limited due to the aircraft or satellite platform vibrations [2]. The purpose of vibration isolation is to isolate the camera system from vibration excitations of the aircraft. The most common type of vibration isolation involves passive [3], active [4], and multistage [5] isolation systems. Generally, vibration experiments are performed to the dynamic characteristics analysis of

the vibration isolator to ensure that the vibrations which cause unfavorable effects on precision systems are isolated. Rashidi and Ziaei-Rad [6] performed quasi-static and dynamic testing to predict the hysteretic behavior of the wire rope isolators. Jong-Seok *et al.* [7] proposed an active mount for the camera systems of a UAV system, and the vibration control performances of the proposed active mount were evaluated in the time and frequency domains through vibration simulation and experiment.

The above vibration measurement systems belong to the mechanical-contact-based method. Recently, in order to meet the requirements to study vibrations without destructing the objects or perturbing the operation of objects, non-contact approaches [8] were studied for vibration measurement by many researchers. Yu *et al.* [9] proposed a single-camera high-speed stereo-digital image correlation method for full-field 3D vibration measurement and dynamic parameters including natural frequencies, damping ratios, and mode shapes of a rectangular cantilever plate were extracted from the directly measured vibration responses. In many vision-based vibration measurement systems, linear array sensors were used to generate sequential image records. Shigang *et al.* [10] used a CCD camera to acquire

the images of the vibrating object and estimated the vibration parameters, e.g., amplitude, frequency, and phase, by applying image processing algorithms to the image data. Zhong *et al.* [11] proposed a vision-based system to measure the rotational speed and vibration of the rotating shaft. In their measurement system the linear array image sensor was used to capture the image sequence of the fringe pattern. Then the video images of the recorded fringe pattern were digitized in gray scales and streamed into the computer through a cable for the estimation of vibration. Tchernykh *et al.* [12] used additional CCD sensors in the focal plane of the satellite camera to measure image motion, and they also performed error analysis of airborne tests in the time domain.

The vibrations caused by engine operation and airflow of the fly platform often vary in amplitude and frequency, which affects the linear array pushbroom aerial cameras by distorting or blurring the image. Over the past years, much research attention has focused on the vibration measurements method based on optical sensors for performance analysis of the vibration isolator or distortions correction. Angular vibration of the aerial survey camera is a major direct cause of limited image distortion and sharpness. Carman [13] proposed an angular vibration measurement flight test method of the aerial camera mounts using Stroboslave electronically flashed lamps. He also performed a laboratory vibration test to measure angular vibration of aerial camera linear vibration using autocollimating telescopes and a plane mirror to provide information on the vibration behavior of aerial cameras under controlled conditions of vibration. In order to accurately simulate the operation conditions of the camera during flight in ground experiments, Janschek *et al.* [14] built up a complete hardware-in-loop test bench to perform analysis of a satellite camera stabilization for real-time image motion measurement. These methods have been performed well in the angular vibration measurements. However, extra external experimental equipments were required by these methods and the operation of them was also costly in man-hours. Therefore, numerical simulations based on the dynamics model of the mechanical system are often performed for the performance analysis of the vibration system [15,16].

In the presented work, the angular vibration of a compact aerial linear array camera was studied. In order to reduce costs and improve efficiency of experiments, we proposed an image-based vibration measurement method for measuring vibration in the remote sensing image in the time and frequency domains directly. By processing the captured aerial images using image segmentation [17] and the Canny edge detection [18] algorithm, the vibration responses were extracted from the distorted image and further used to analyze the dynamic parameters of the angular vibration. Also, the operating vibration conditions of the aircraft including a MI-171 helicopter, Nanchang Y-5, and a UAV system were measured to study the vibration characteristics of the platform. Different from the method proposed by [13,14], the digital images captured by the linear array camera itself are used for the vibration measurement in the time and frequency domains, making it attractive for the operating condition monitoring and performance analysis of the aerial camera.

In the next section the camera system studied in this paper is introduced and the vibration conditions of the aircrafts carrying

this camera are also described. Section 3 introduces the image-based vibration measurement method proposed by this paper. Detailed results of the flight tests and performance analysis are given in Section 4. The conclusions are presented in Section 5.

## 2. VIBRATION CONDITIONS MEASUREMENTS

### A. Camera Description

The aerial camera studied in this paper consists of a lens, focal plane component, thermal control component, position and orientation system (POS), stable platform, and mechanical vibration isolation, as shown in Fig. 1(a). The coordinate used in this paper is illustrated in Fig. 1(b); X, Y, and Z are, respectively, the longitudinal, lateral, and vertical directions of the aircraft. The parameters of the camera are shown in Table 1. The stabilized platform uses the inertial measurement unit to measure the low-frequency vibrations caused by the change of aircraft attitude and compensates the camera body externally via gimbal counter motions. The mechanical vibration isolation isolates the high-frequency vibration that mainly caused by engine operation. The POS provides the six dimensions location and orientation information of the camera at every exposure time which are used in the image post-processing.

### B. Vibration Isolation System

The necessary background on vibration theory is briefly summarized here [19]. For a single-degree-of-freedom vibration system, the mathematical formula of motion of mass  $m$  is

$$m\ddot{x} + c\dot{x} + kx = F(t), \quad (1)$$

where  $c$  and  $k$  are respectively known as the damping and stiffness coefficients, and  $F(t)$  denotes the excitation force.

If we neglect damping, the natural frequency of the system is

$$f_n = \frac{1}{2\pi} \sqrt{\frac{k}{m}}, \quad (2)$$

and transmissibility is the ratio of transmitted force to the input force  $F_0$  as

$$T = \left| \frac{F(t)}{F_0} \right|. \quad (3)$$

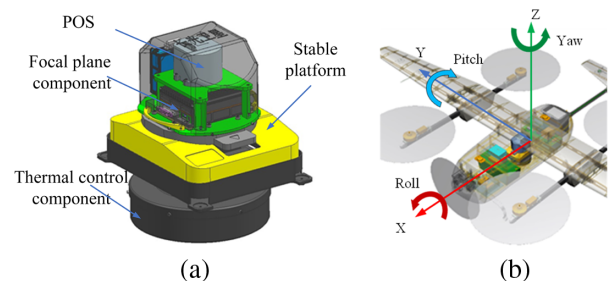
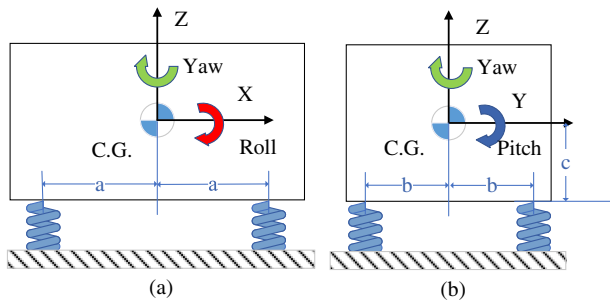


Fig. 1. Description of the camera: (a) camera, (b) UAV system.

Table 1. Parameters of the Camera

Imaging Mode	Mass	Size	Focal Length
Pushbroom	12 kg	320 L × 252 W × 345 H	40 mm



**Fig. 2.** Diagram of camera mount: (a) front view, (b) lateral view.

Transmissibility  $T$  reaches its maximum value when excitation frequency  $\omega$  is equal to  $f_n$ . In the region where  $0 < \omega < \sqrt{2}f_n$ , vibration is amplified and  $T > 1$ . Whereas in the region  $\omega > \sqrt{2}f_n$ , vibration is isolated ( $T < 1$ ) and the isolation effectiveness  $I = (1 - T) \times 100\%$  [20]. Generally, a soft vibration isolation can be helpful to isolate the linear vibration because it provides low resonance frequency of the isolation system and thus reduces the frequency band of vibration amplification. However, a soft vibration isolation can cause very large displacement under conditions of excessive disturbance, such as landing or camera buffeting by airflow. For minimum transmissibility (maximum isolation effectiveness), the excitation frequency should be as high above the natural frequency as possible. Therefore, the natural frequency of isolation mount of a large aerial camera (weight  $> 100$  kg) is always below 10 Hz [13]. However, considering the weight of the compact camera is about 10 kg, if the system stiffness is less than 30 Hz, it will result in a very low system stiffness. Then, the natural frequency of the rubber isolators is designed as 35 Hz in all three directions.

The camera mount in the aircraft coordinate system was shown in Fig. 2. The XZ and YZ planes are planes of symmetry. The rubber isolators are identical and are located symmetrically about the Z axis. The rotations of the camera about these axes are indicated by  $\alpha$  (roll),  $\beta$  (pitch), and  $\gamma$  (yaw).

**C. Vibration Conditions**

It is generally known that the measurement of the aircraft’s vibration conditions is very important as a typical first step to develop an effective vibration isolation for an aerial camera. Therefore, in this work the vibrations of the aerial vehicles including a MI-171 helicopter, Nanchang Y-5, and a fixed-wing UAV system, which are the potential carriers of the camera in the future, were measured. The UAV system used in this experiment was the G45 UAV provided by Changguang satellite technology company. The experimental setup for vibration measurement is shown in Fig. 3. The translational vibrations of the camera’s installation position were measured in three directions during the flight test. Then the recorded vibration data were processed in the time and frequency domains after the flight test. Figure 4 shows the time and frequency vibration in the Z direction of the Nanchang Y-5.

Table 2 summarizes the vibration measurement data of the three different aerial vehicles in flight tests, in which the resonance vibration frequency and amplitude in the Z direction are given. A high-amplitude–high-frequency vibration condition

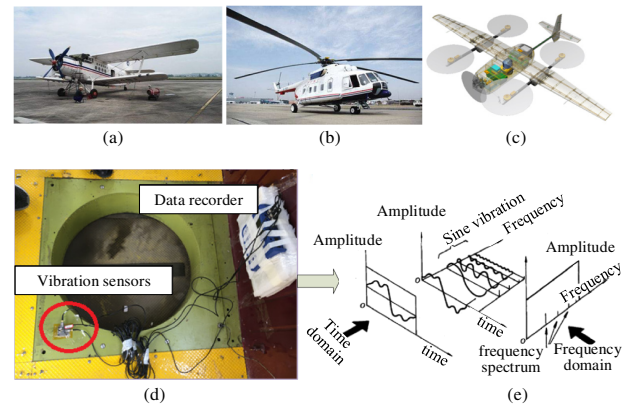


**Fig. 3.** Vibration measurements of aircraft setup: (a) Nanchang Y-5, (b) MI-171, (c) UAV system, (d) vibration measurement device, (e) data processing.

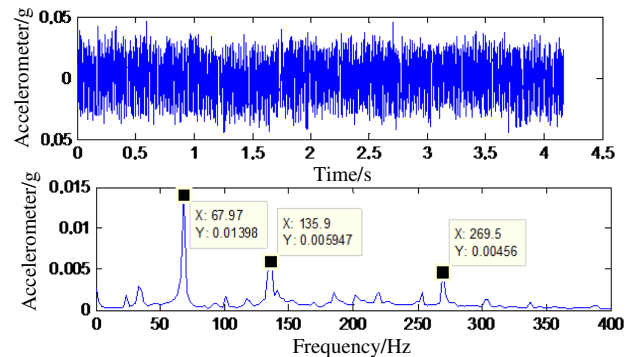


**Fig. 4.** Vibration conditions of Nanchang Y-5.

**Table 2. Vibration Conditions**

Aircraft	G45UAV	MI-171	Nanchang Y-5
Type	Fixed-wing	Helicopter	Fixed-wing
Takeoff weight	45 kg	13,011 kg	5250 kg
Engine type	Piston	Turboshaft	Piston
Cruise speed	100 km/h	240 km/h	160 km/h
Excitation frequency	92.5 Hz	16 Hz	68 Hz

(92.5 Hz, 0.19 g) was observed in the G45 UAV flight experiment, which was the worst vibration condition for the camera. Moreover, a low-amplitude–low-frequency vibration condition (16 Hz, 0.001 g) was observed in the MI-171 flight experiment, which may require very-low-frequency isolators.

**3. IMAGE-BASED VIBRATION MEASUREMENT METHOD**

**A. Measurement Principle**

Pushbroom sensors are commonly used in space and aerial cameras. The pushbroom sensors are mounted on the flight platform and perpendicular to the flight direction. As the platform moves, the sensor array sweeps out a region of space in the flight direction. At regular intervals of time one-dimensional images (1D) of the view plane are captured. Then, the ensemble of these 1D images constitutes a two-dimensional (2D) image. For the aerial

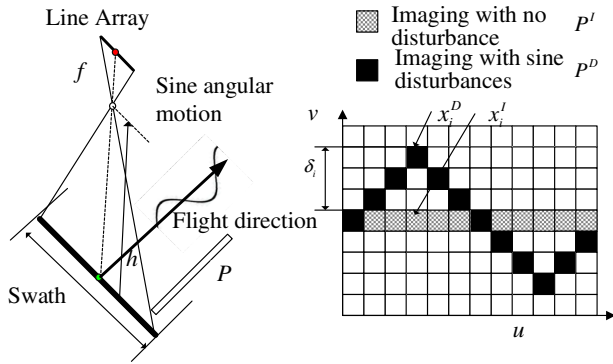


**Fig. 5.** Image motion measurement.

camera studied in this paper, the linear array of sensors consists of 12,000 pixels of electronic sensors.

Figure 5 shows the principle of image motion (displacement) measurement of vibration based on the pushbroom sensors. For a linear object  $P$  that is parallel to the flight direction on the ground, its image  $P^I$  captured by the camera will be a straight line if the camera is not influenced by external disturbances during the imaging process. However, if the external disturbance causes the attitude motion of the camera, such as a sinusoidal disturbance along the rolling direction, the image  $P^D$  will be a sinusoidal curve. The image of an arbitrary point  $x_i$  of  $P$  in the  $i$ th linear image is described by two coordinates. The first coordinate  $u$  represents the row number of the  $i$ th image, and the second coordinate  $v$  represents the projection of the point on the image line. The image motion  $\delta_i$  and time  $t_i$  could be expressed as

$$\delta_i = v_i^I - v_i^D, \quad (4)$$

$$t_i = t_s \times u_i, \quad (5)$$

where  $v_i^I$  and  $v_i^D$  represent the pixel positions of point  $x_i$  of images  $P^I$  and  $P^D$ , respectively, in the  $i$ th 1D image;  $t_s$  is the exposure time of every linear image.

The angular vibration, especially the angular vibration in roll, is the main cause of image distortion. The relation of image motion and roll angle of the camera could be written as

$$\delta(t) = f \tan \alpha(t), \quad (6)$$

where  $f$  is the focal length of the camera and  $\alpha(t)$  is the roll angle of the camera.

The procedures to determine the image motion and to analyze vibration in the time and frequency domains are summarized into three steps, as illustrated in Fig. 6. First, a flight test is performed. Both the camera and vibration sensors are mounted on the platform to record the image and linear vibration, respectively. The raw images of the linear sensor are constituted to a 2D image based on time-reference sequential. Second, the objects with a linear edge are selected from the 2D image. The image segments of these objects are then extracted and further processed to edge detection using image processing technology. Then, by calculating the image motion of the extracted edge using the proposed method above, the time-displacement results can be determined. Finally, these resulted

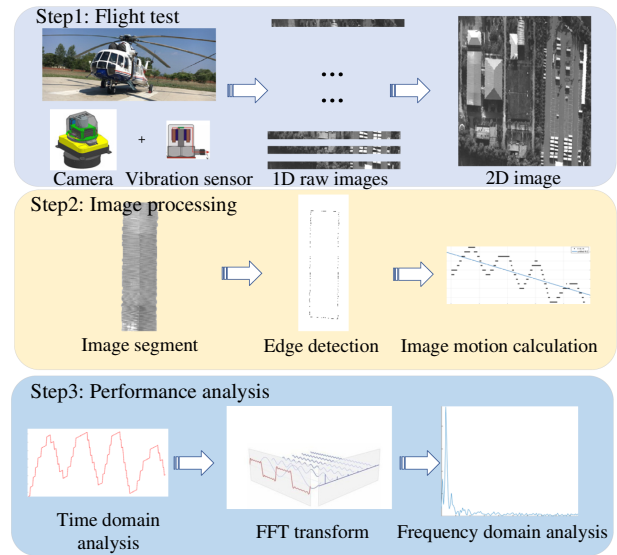


**Fig. 6.** Procedures of the image-based method.

time-displacement responses are processed using the fast Fourier transform (FFT).

## B. Image Processing Method

Among the three steps, the image processing is the key step for acquiring the input data for vibration analysis. Generally, the edges of the road, house, and parking line, etc., are approximately linear. The threshold method [21] is used for image segmentation of the projection of these objects on the image for the images including these objects often have a relative high level of contrast. The image is converted to a binary image as the following equation:

$$g(u, v) = \begin{cases} 1, & \text{if } f(u, v) > T \\ 0, & \text{if } f(u, v) \leq T \end{cases}, \quad (7)$$

where  $T$  represents the threshold;  $f(u, v)$  is the gray value of pixel  $(u, v)$ ; and  $g(u, v)$  is the threshold version of  $f(u, v)$ .

The binary image should contain all the essential information about the position and shape of the objects of interest (foreground). Therefore, the value of threshold  $T$  is the key parameter of the threshold method and the thresholding algorithm of calculation  $T$  is introduced in [22].

To significantly reduce the amount of data in the foreground image, while accurately preserving the structural properties to be used for further vibration analysis, the Canny edge detection method is utilized to extract the distorted features from the foreground image. More details about the Canny edge detection methods can be found in [18]. The extracted results are defined by pixel coordinate  $(u, v)$  and thus converted to time-pixel coordinates  $(t, v)$ . Finally, the results  $(t, v)$  are used to reconstruct the edge of the object at undistorted state according to the first-order polynomial fitting method as

$$H(t) = at + b, \quad (8)$$

where  $H(t)$  is the formulation of the undistorted object and coefficients  $a$  and  $b$  are identified by the polynomial fitting method.

Then the image motion in the time domain could be expressed as

$$z(t_i) = v_i - H(t_i). \tag{9}$$

### 4. EXPERIMENTS

#### A. Laboratory Vibration Test

To provide information on the vibrational behavior of the aerial camera under controlled conditions, the camera vibration isolation was tested on large laboratory shakers [8]. The shaker provided strictly linear vibration of controlled amplitude and frequency in either a vertical or horizontal direction, as shown in Fig. 7. Sensors 1 and 3 were mounted on the camera to measure the vibration response of the camera, and sensor 2 was mounted on the mechanical mount base to measure the vibration input. On the base of the preliminary aircraft vibration test, the applied sinusoidal linear vibration was given 0.1 g amplitude from 10 Hz to 300 Hz.

For each of the three directions of applied sinusoidal vibration, the linear vibrations were measured as components in the X, Y, and Z directions. Figure 8 shows the frequency results of sensors 1 and 2 in the Z directional vibration test. The vibration isolation's resonance frequency is 35 Hz, and the amplitude of sensor 1 is less than that of sensor 2 when the frequency is greater than about 60 Hz. Therefore, the excitation frequency of MI-171 (16 Hz) is in the amplified region, and the excitation frequencies of G45 UAV (92.5 Hz) and Nanchang Y-5 (68 Hz) are in the isolated region. Table 3 gives a summary of the laboratory vibration test results, and the transmissibility corresponding to the excitation frequency of the three aircrafts is also given. The difference of the resonance frequency in the three directions could be related to the installation accuracy and damping. The isolation system achieves 42% isolation efficiency at 68 Hz and 67% at 92.5 Hz. However, the isolation system is as a vibration amplifier rather than as vibration isolation at the resonance frequency of MI-171.

#### B. Flight Experimental Setup

To verify the performance of the vibration isolation and the method proposed in this paper, a flight experiment setup using a MI171 helicopter was developed, as illustrated in Fig. 9. The experimental system includes a camera system, translational vibration measurement (three vibration sensors), mount base,

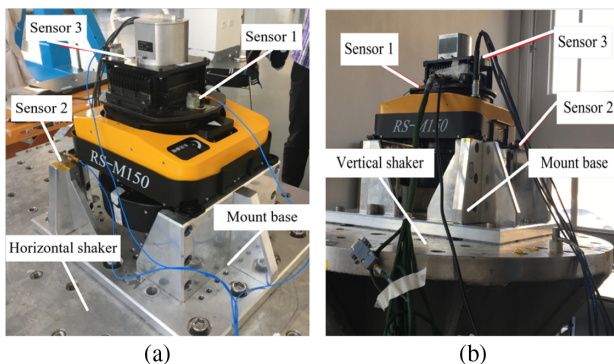


Fig. 7. Laboratory test of vibration isolation system. (a) X/Y direction, (b) Z direction.

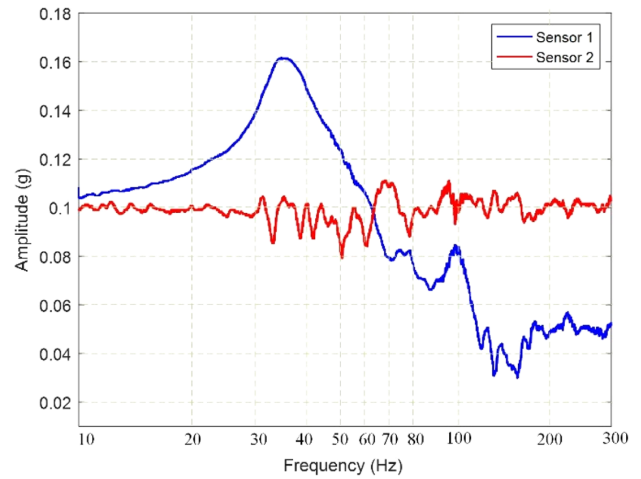


Fig. 8. Frequency results of vibration test in Z.

Table 3. Laboratory Test Results

Direction	Natural Frequency	Transmissibility T		
		16 Hz	68 Hz	92.5 Hz
X	29.5	142%	25%	15%
Y	32	128%	50%	20%
Z	35	134%	58%	33%

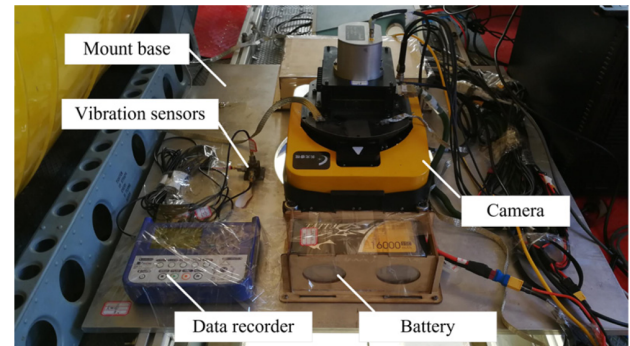


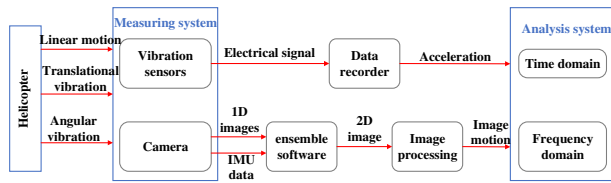
Fig. 9. Flight experiment.

Table 4. Flight Parameters

Ground Resolution	Velocity	Altitude	Rount Spacing	Rount Length
0.1 m	170 km/h	727 m	780 m	15 km

power supply system, and a computer. Note that, the mount base with high natural frequency and assembly accuracy is critical to ensure the parallelism of the coordinates of the translational vibration sensors, camera, and helicopter. The flight parameters of the helicopter are shown in Table 4. Totally, the survey area was 40 km<sup>2</sup>.

The main data flows of the flight experiment are shown in Fig. 10. The translational vibrations input of the camera were directly obtained by the vibration measuring system. The image vibrations were obtained by the camera and processed by the proposed measurement system.



**Fig. 10.** Data flows of flight experiment.



**Fig. 11.** 2D panchromatic image.

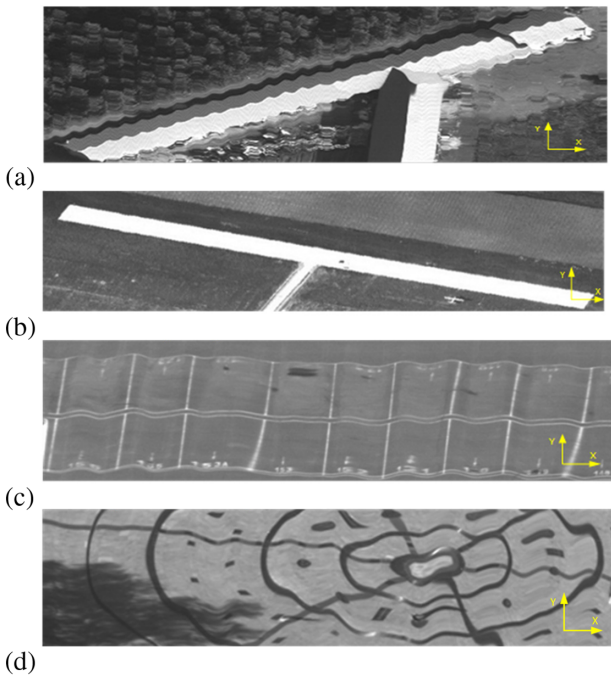


**Fig. 12.** Image segments: (a) Case 1, house image; (b) Case 2, runway image; (c) Case 3, parking line image; (d) Case 4, complex pattern image.

### C. Image Processing Results

The 2D image was constituted by the ensemble of 1D raw linear images in time reference sequence, as shown in Fig. 11. Image segments of the 2D image were extracted for image processing. As shown in Fig. 12, these image segments are the images of a house, runway, parking line, and complex pattern. The image resolutions of Cases 1, 2, 3, and 4 are  $1270 \times 1989$ ,  $99 \times 2545$ ,  $2828 \times 11215$ , and  $1383 \times 313$  pixels, respectively. It is apparent that the linear objects were distorted in these images. It is apparent in these images that the intensity distribution between the objects of foreground and background are very distinct. Therefore, it is easy to perform foreground segmentation using the threshold method.

However, in order to obtain the pixel-scale displacement accuracy, the value of threshold was optimized in each case to a higher precision of the shape of the foreground. The foreground segmentation images were directly processed into black-and-white high-contrast images for convenience of edge detection, as shown in Figs. 13–16(a). The Canny detector performed well to extract the edges from the foreground segmentations and the width of these edges was one pixel-scale. Note that the edges of the foreground image were “the images of edge,” which means that they were defined in pixel coordinate. In Fig. 15(a), the image motion along the flight direction can be observed (red dotted area) which is caused by the pitch angular vibration. However, the time-displacement curve of the pitch angular vibration cannot be obtained by the proposed method for the imaging time of the analyzed region can only be deduced by the number of frames in the pushbroom direction and the exposure time of each frame.

Then the distorted curves (blue dotted area) were transformed into the time domain as illustrated in Figs. 13–16(b). The initial time was assumed to be the exposure time of the first linear image of the segment. The column pixel coordinate of the edge was translated as

$$y(i) = y(i) - \sum_1^n y(i)/n, \quad (10)$$

where  $y(i)$  is the column pixel coordinate of linear image  $i$ , and  $n$  represents the number of the linear images.

### D. Data Processing

In the ideal conditions (without disturbance), the edges of these foreground images can be approximate to a straight line. However, the extracted edges were distorted due to the attitude instability and vibrations. To determine the frequency of external disturbance recorded in the image, displacement of the foreground image should be first extracted. Moreover, to further demonstrate the performance of the proposed method in vibration measurement, the roll angle recorded by the POS was extracted and processed. Figure 17(a) shows the roll angle in the time domains of POS data corresponding to Case 1. The recorded roll angle data were transformed into image motion according to the projection Eq. (6), and the displacements of the foreground image were extracted according Eqs. (4) and (5), as shown in Fig. 17(b).

By processing these displacements data using the FFT, the resonant frequencies of the disturbance can be extracted from the FFT spectrums, as shown in Figs. 18–21. The low disturbance frequencies ( $<10$  Hz) with relatively large amplitudes were mainly caused by the change of aircraft attitude, for we have known that the vibration frequency of MI-171 caused by the engine is about 16 Hz from Table 2. In order to focus on the analysis of image displacement caused by vibration, a high-pass filter was used to filter the results. For brevity, details of the high-pass filter are not given here.

To investigate the performance of the proposed method, the recorded vibration sensors were also analyzed for comparison. The raw recorded data in three directions of the vibration sensors are shown in Fig. 22. These data were processed using

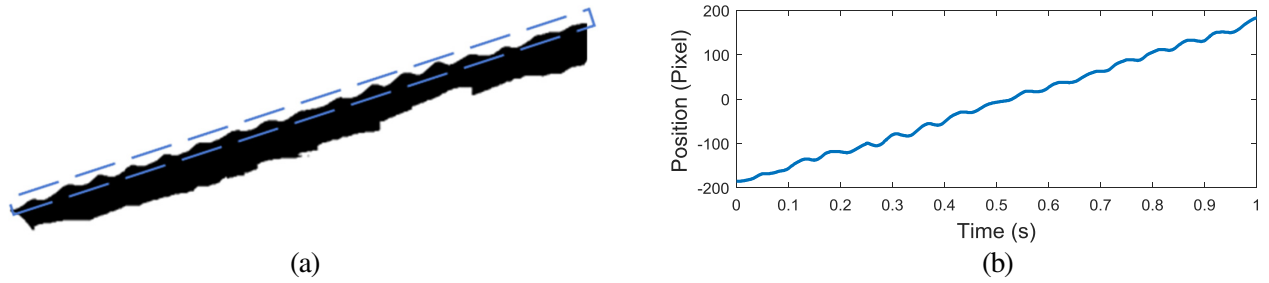


Fig. 13. Image processing results of Case 1: (a) foreground image, (b) edge detection.

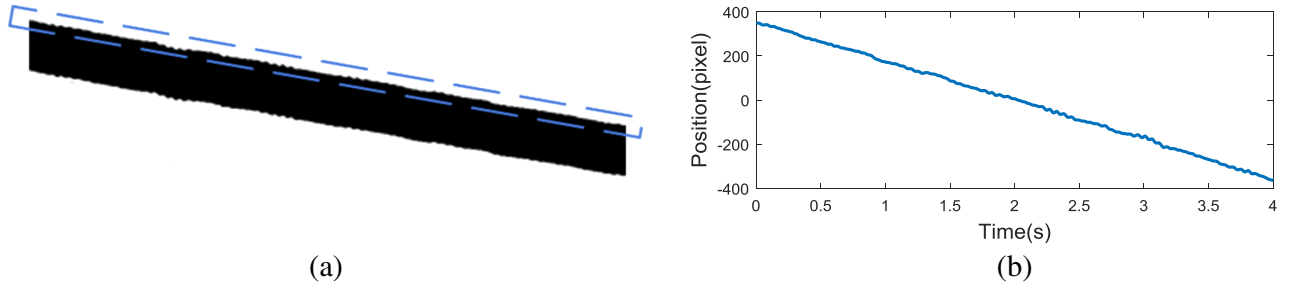


Fig. 14. Image processing results of Case 2: (a) foreground image, (b) edge detection.

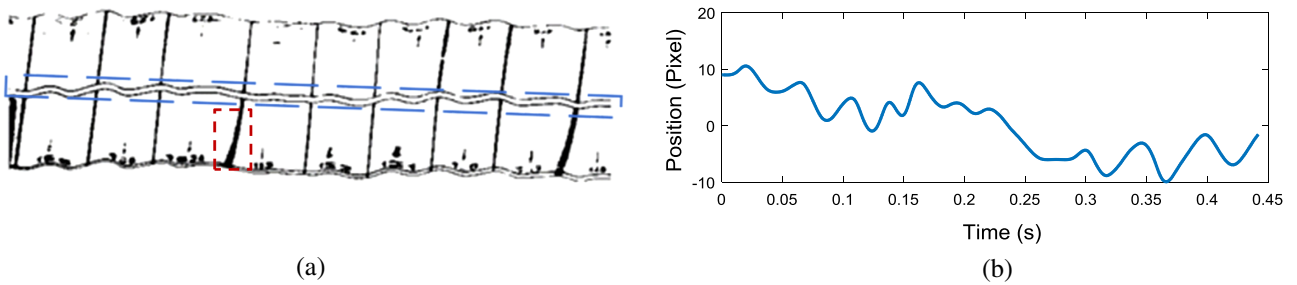


Fig. 15. Image processing results of Case 3: (a) foreground image, (b) edge detection.

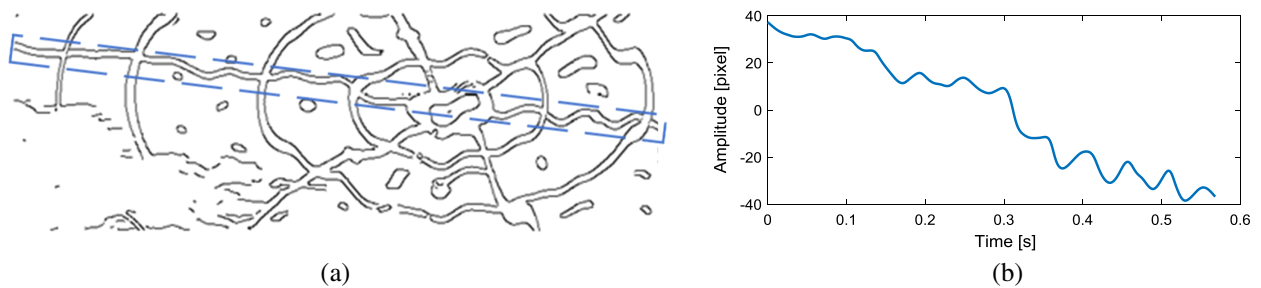
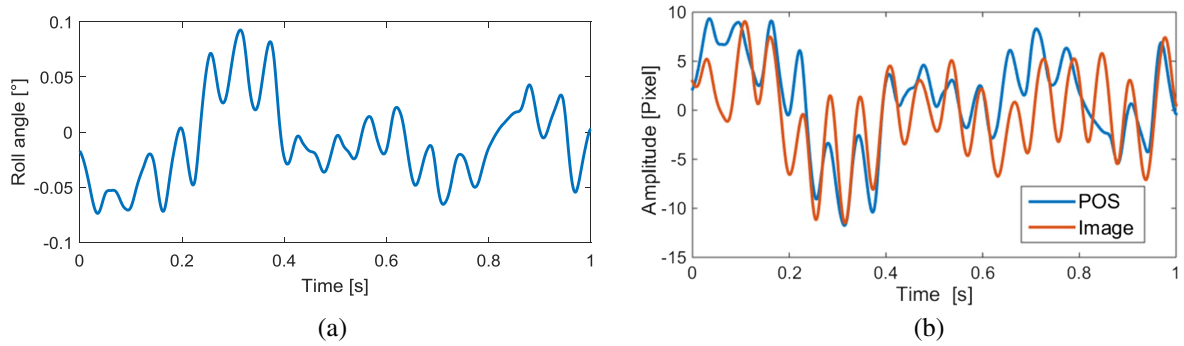


Fig. 16. Image processing results of Case 4: (a) foreground image, (b) edge detection.

the FFT, and the results are shown in Table 5. For the periodic vibrations were produced by the mechanical excitations of the rotating propeller and reciprocating engines operating with a constant rotational speed; three harmonic response peaks were observed. The harmonic frequencies are 16.4 Hz, 32.2 Hz, and 48.4 Hz, respectively, which were caused by the engine operation. The first-order vibration frequency of the engine during the whole flight process is 16.4 Hz. The 341.8 Hz is the natural frequency of the mount base.

### E. Error Analysis

In order to analyze the relationship between the frequency domain results of the POS and image processing, the frequency distribution histogram of these results is illustrated in Fig. 23. The measured vibration frequency range is 15 Hz to 19 Hz, which are consistent with the vibration frequency measured by the vibration sensors, and the frequency difference between them was mainly caused by the change of cruising speed (engine speed) in different flight stages.



**Fig. 17.** POS data of Case 1: (a) POS data, (b) amplitude of POS and image calculation.

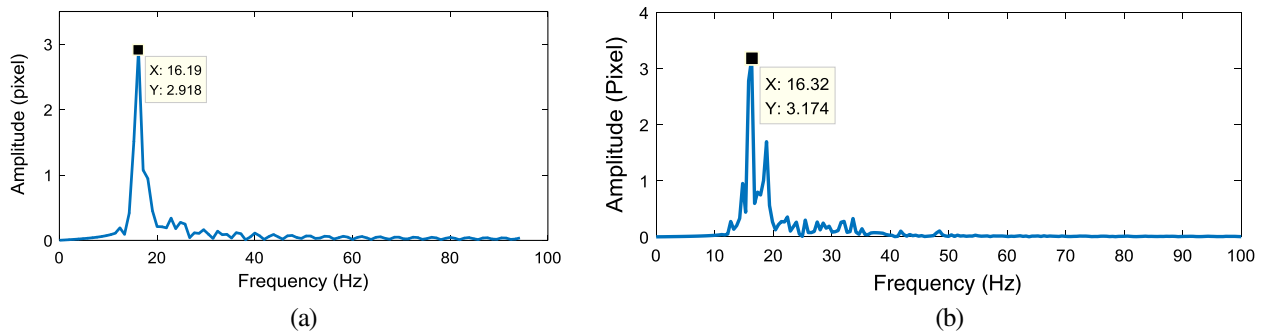


**Fig. 18.** Results in frequency domain of Case 1: (a) image method, (b) POS.

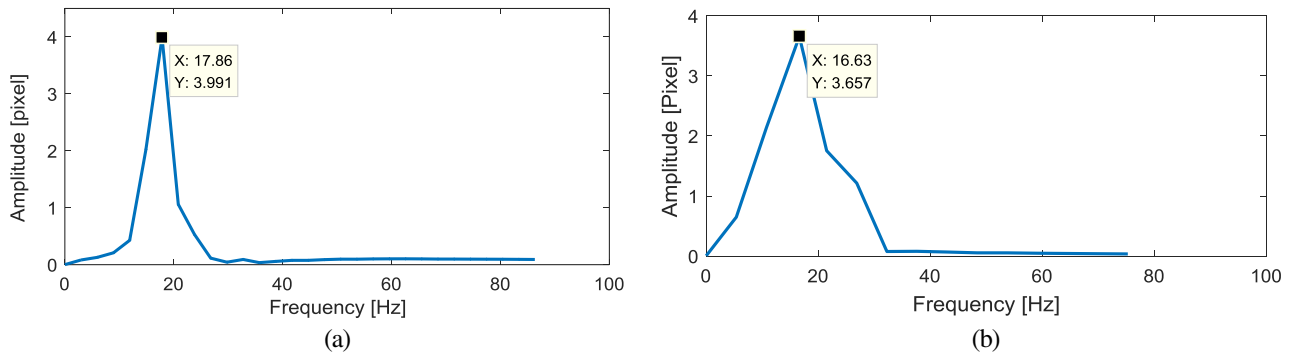


**Fig. 19.** Results in the frequency domain of Case 2: (a) image method, (b) POS.

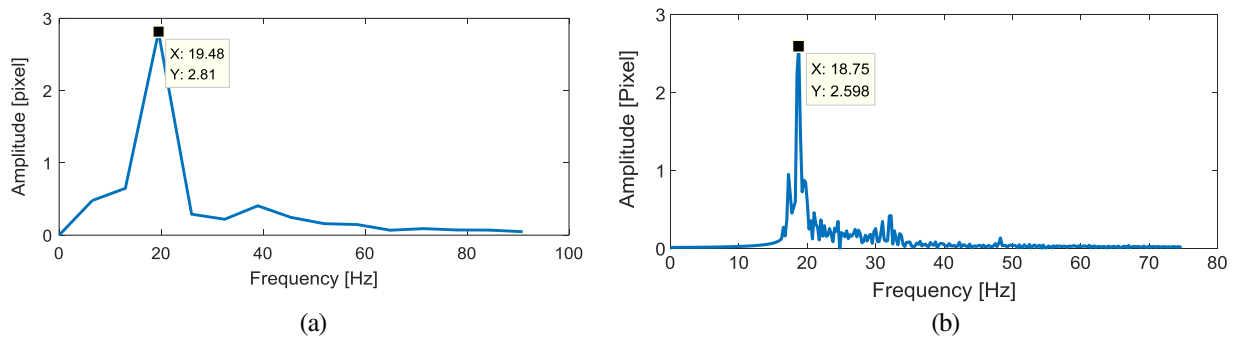


**Fig. 20.** Results in the frequency domain of Case 3: (a) Image method, (b) POS.

Table 6 shows the frequency results comparison of image processing and POS data of Cases 1–4. A good agreement (errors less than 10%) can be observed between the frequency

and amplitude results of the image processing method and POS data. Moreover, the edge curve in the foreground image of Case 4 is discontinuous, and the curve was smoothed after edge

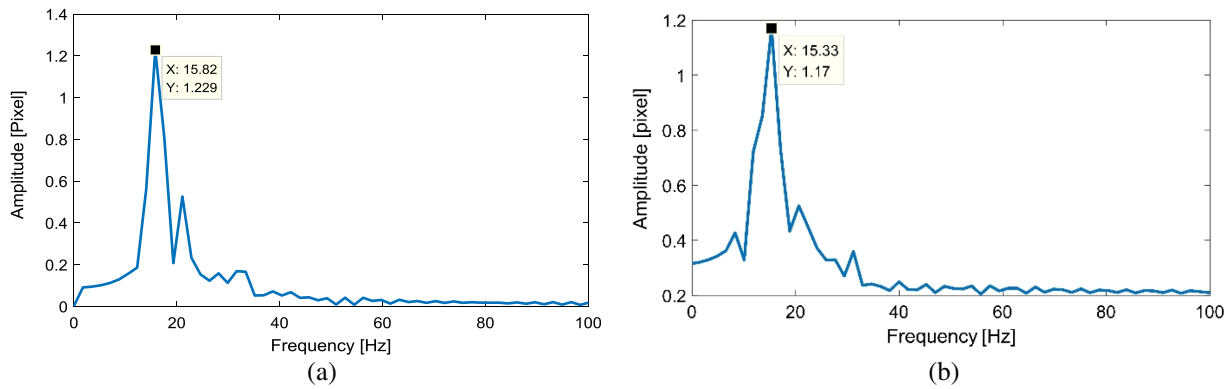


Fig. 21. Results in the frequency domain of Case 4: (a) Image method, (b) POS.

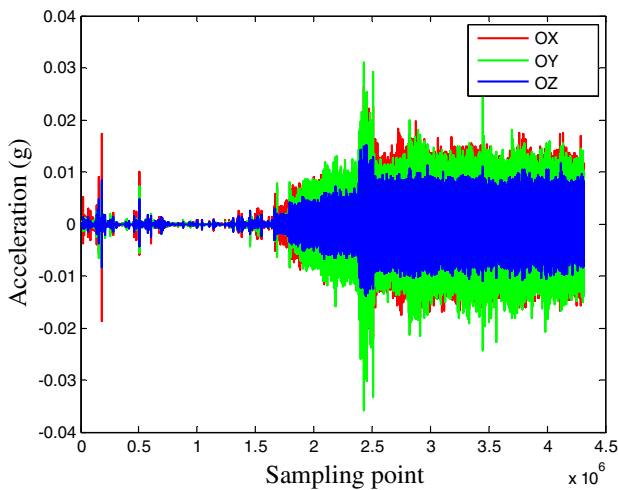


Fig. 22. Raw data of vibration sensors.

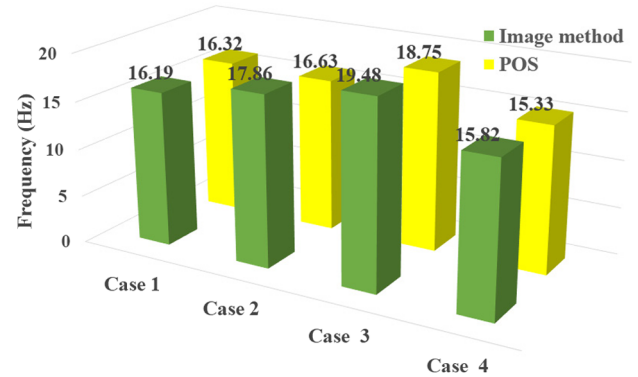


Fig. 23. Frequency distribution histograms.

Table 5. Frequency Results of Vibration Sensors

Resonance Frequency	Amplitude (g)		
	X	Y	Z
16.4 Hz	0.0018	0.0014	0.0016
32.2 Hz	0.0015	0.0008	0.0012
48.4 Hz	0.0005	0.0015	0.0003
341.8 Hz	0.0027	0.0006	0.0008

Table 6. Comparison of Results

Case	Data	Image	POS	Errors
1	Frequency (Hz)	16.19	16.32	0.8%
	Amplitudes (Pixel)	2.918	3.174	8.1%
2	Frequency (Hz)	17.86	16.63	7.39%
	Amplitudes (Pixel)	3.991	3.657	9.1%
3	Frequency (Hz)	19.48	18.75	3.9%
	Amplitudes (Pixel)	2.81	2.598	8.2%
4	Frequency (Hz)	15.82	15.33	3.2%
	Amplitudes (Pixel)	1.229	1.17	5.0%

detection, as shown in Fig. 16. The image processing method also offers very good accuracy in Case 4.

### 5. CONCLUSIONS

In this study, an image-based method using the aerial image and image processing technology is proposed for the vibration measurement of a linear array camera. The effectiveness and accuracy of the proposed approach were verified by the flight test. Moreover, the results of the proposed method, vibration sensors, and POS are compared. Based on the results of this study, the following main conclusions can be drawn:

- (1) One of the key properties of the image-based method is that it focuses on the analysis of the image acquired by the camera itself after flight missions. Therefore, the measurement results of the proposed method represent the vibration conditions of the camera under actual operational environment.
- (2) The key step of the proposed method consists in calculating the image motion from the image segments by the image processing method. Both the threshold method and the Canny edge detection method were used to extract the distortion curve of the object from the image with pixel-scale displacement accuracy. The accuracy of the proposed method does not improve significantly when other image processing methods are used.
- (3) The comparison of the results of the image-based method, vibration sensors, and POS of the flight experiment shows an acceptable accuracy of the proposed method. A time synchronization system including the image, vibration sensor, POS, and engine signal is needed for a more detailed

performance analysis of the proposed method in the future. Note that this approach is not intended to replace the POS. It provides an effective means for image motion analysis based on aerospace images to determine the vibration source of image disturbance.

- (4) A limitation of this study is that only the angular vibration in the roll directional can be measured. Moreover, the proposed method is not suitable for application in the very-high-frequency vibration measurements such as the image motion measurement during the exposing time.

Generally speaking, we observe that the image-based method proposed in this paper effectively offers good potential to be applied to other aerial or space linear array cameras for performance analysis of image quality or vibration isolation system.

**Funding.** Department of Science and Technology of Jilin Province (20170201006GX, 20170204078GX, 20180201106GX).

**Disclosures.** The authors declare no conflicts of interest.

## REFERENCES

1. J. Windau and L. Itti, "Multilayer real-time video image stabilization," in *IEEE/RSJ International Conference on Intelligent Robots and Systems* (2011), pp. 2397–2402.
2. J. Haghshenas, "Vibration effects on remote sensing satellite images," *Adv. Aircraft Spacecr. Sci.* **4**, 543 (2017).
3. Y. Yu, N. G. Naganathan, and R. V. Dukkipati, "A literature review of automotive vehicle engine mounting systems," *Mech. Mach. Theory* **36**, 123–142 (2001).
4. T. Sato and D. L. Trumper, "A novel single degree-of-freedom active vibration isolation system," in *Proceedings of the 8th International Symposium on Magnetic Bearing* (2002).
5. F. Matichard, B. Lantz, K. Mason, R. Mittleman, B. Abbott, S. Abbott, E. Allwine, S. Barnum, J. Birch, and S. Biscans, "Advanced LIGO two-stage twelve-axis vibration isolation and positioning platform. Part 1: design and production overview," *Precis. Eng.* **40**, 273–286 (2015).
6. S. Rashidi and S. Ziaei-Rad, "Experimental and numerical vibration analysis of wire rope isolators under quasi-static and dynamic loadings," *Eng. Struct.* **148**, 328–339 (2017).
7. J.-S. Oh, Y.-M. Han, and S.-B. Choi, "Vibration control of a camera mount system for an unmanned aerial vehicle using piezostack actuators," *Smart Mater. Struct.* **20**, 085020 (2011).
8. P. S. Harvey, Jr., G. Elisha, and C. D. Casey, "Experimental investigation of an impact-based, dual-mode vibration isolator/absorber system," *Int. J. Non Linear Mech.* **104**, 59–66 (2018).
9. L. Yu and B. Pan, "Single-camera high-speed stereo-digital image correlation for full-field vibration measurement," *Mech. Syst. Sig. Process.* **94**, 374–383 (2017).
10. S. Wang, B. Guan, G. Wang, and Q. Li, "Measurement of sinusoidal vibration from motion blurred images," *Pattern Recognit. Lett.* **28**, 1029–1040 (2007).
11. J. Zhong, S. Zhong, Q. Zhang, N. Maia, Y. Shen, S. Liu, Y. Yu, and Z. Peng, "Vision-based system for simultaneous monitoring of shaft rotational speed and axial vibration using non-projection composite fringe pattern," *Mech. Syst. Sig. Process.* **120**, 765–776 (2019).
12. V. Tcherykh, S. Dyblenko, K. Janschek, K. Seifart, and B. Harnisch, "Airborne test results for smart pushbroom imaging system with optoelectronic image correction," *Proc. SPIE* **5234**, 550–559 (2004).
13. P. D. Carman, "Aerial camera vibration," *Photogramm. Eng. Remote Sens.* **48**, 1845–1856 (1982).
14. K. Janschek, V. Tcherykh, and S. Dyblenko, "Performance analysis of opto-mechatronic image stabilization for a compact space camera," *Control Eng. Pract.* **15**, 333–347 (2007).
15. A. Tamer, V. Muscarello, P. Masarati, and G. Quaranta, "Evaluation of vibration reduction devices for helicopter ride quality improvement," *Aerosp. Sci. Technol.* **95**, 105456 (2019).
16. Y. Zhang, C. Sheng, Q. Hu, M. Li, Z. Guo, and R. Qi, "Dynamic analysis and control application of vibration isolation system with magnetic suspension on satellites," *Aerosp. Sci. Technol.* **75**, 99–114 (2018).
17. M. F. Talu, "ORACM: online region-based active contour model," *Expert Syst. Appl.* **40**, 6233–6240 (2013).
18. J. Canny, "A computational approach to edge detection," *IEEE Trans. Pattern Anal. Mach. Intell.* **PAMI-8**, 679–698 (1986).
19. C. M. Harris and A. G. Piersol, *Harris' Shock and Vibration Handbook* (McGraw-Hill, 2002), Vol. **5**.
20. M. L. M. Duarte and J. A. Fernandes, "Measurement of vibration transmissibility for continuous systems," *Inverse Prob. Des. Optim.* **2**, 215 (2005).
21. N. Kaur and R. Kaur, "A review on various methods of image thresholding," *Int. J. Comput. Sci. Eng.* **3**, 3441 (2011).
22. M. S. Priya and D. G. K. Nawaz, "Multilevel image thresholding using OTSU's algorithm in image segmentation," *Int. J. Sci. Eng. Res.* **8**, 101–106 (2017).